

In-situ electro-optic sampling of microwave signals under cryogenic conditions and for superconducting applications

Shekhar Priyadarshi¹, Oliver Kieler¹, Alexander Fernandez Scarioni¹, Judith Felgner¹, Abdulrahman Widaa¹, Johannes Kohlmann¹, Thomas Fordell², Jaani Nissilä², Antti Kemppinen², and Mark Bieler¹

¹ Physikalisch-Technische Bundesanstalt, Bundesallee 100, 38116 Braunschweig, Germany.

² VTT Technical Research Centre of Finland Ltd, 02150 Espoo, Finland.

Corresponding author: mark.bieler@ptb.de.

Abstract — We demonstrate a cryogenic electro-optic sampling (EOS) setup that allows for the measurement of microwave signals at arbitrary positions on a cryogenic chip-scale device. We use a Josephson Arbitrary Waveform Synthesizer (JAWS) to generate quantum-accurate voltage signals and measure them with the EOS setup, allowing for the calibration of its response, yielding traceability of the microwave measurements to a quantum standard. We use the EOS setup to determine the time-domain response of ultrafast cryogenic photodiodes and the electrical reflection coefficient, i.e., the S_{11} scattering parameter, in a superconducting transmission line. Finally, we introduce an optical femtosecond pulse source which can be used to study the fidelity of superconducting transmission lines and terminations, as well as reflections from elements like Josephson junction arrays imbedded in them.

Index Terms — Ultrashort voltage pulse, electro-optic sampling, photodiode characterization, Josephson Arbitrary Waveform Synthesizer (JAWS), cryogenic temperature, fiber-chip coupling, pulsed laser.

I. INTRODUCTION

All solid-state approaches for quantum computing and many other quantum technologies rely on microwave signals [1], [2]. These experiments are typically black boxes, i.e., there is only indirect information about the microwave signal levels and purity. One of the problems is a tradeoff between thermal insulation and bandwidth of metallic cables that carry microwave signals from the cryogenic devices to room temperature measurement electronics. Hence such cables have significant losses already around 1 GHz. In particular, none of the conventional methods allow reliable time-domain, oscilloscope-like measurements of cryogenic signals in the interesting frequency range between 1 GHz and 1 THz [3], [4], [5].

Unlike electrical cables, optical fibers have simultaneously wide bandwidth and low thermal conductivity, which has raised the interest, e.g., in the opto-electrical control and readout of quantum computers and other quantum technologies [6], [7]. One of the promising approaches for cryogenic signal generation is the Josephson Arbitrary Waveform Synthesizer (JAWS) that can also be driven optically, and its variant, the Josephson Pulse Generator (JPG), that already enabled qubit control [8], [9].

Recently, we demonstrated electro-optic sampling (EOS) of a cryogenic photodiode [10], where laser-based measurements and optical fibers offer a very high bandwidth, which easily exceeds 1 THz, and allow for low-invasive and in-situ measurements. One interesting application for this setup is to study electric pulse propagation in superconducting circuits such as JAWS, which is sensitive to signal reflections [11], [12]. Here we report on a reversed experiment, where JAWS is used as a quantized reference signal source that allows the calibration of the EOS sampling setup.

We like to note that this manuscript is an extension of a conference proceedings paper [13], yet, with significantly enhanced content. While the order of Secs. IV and V has been reversed, Secs. VI and VII are newly added to this manuscript, which is structured as follows. In Sec. II we introduce the EOS setup based on femtosecond lasers. In Sec. III we utilize the setup for the characterization of commercially available photodiodes with nominal bandwidths of 60 GHz and compare their responses at room temperature and at cryogenic temperature. We extend the EOS setup in Sec. IV to measurements of electrical reflection coefficients, corresponding to S_{11} scattering parameter measurements. We then use a JAWS to calibrate the EOS setup to a quantum standard in Sec. V and measure the JAWS output at cryogenic temperatures in the time-domain in Sec. VI. Finally, we

introduce the direct EOS of an optical pulse pattern generator in Sec. VII before we conclude in Sec. VIII.

II. EXPERIMENTAL SETUP

The main part of the experimental setup is shown in Fig. 1. Different types of commercially available p-i-n photodiodes (PD) are flip-chip bonded to one end of a coplanar waveguide (CPW), which is made of either Nb or Au. For the optical excitation of the PDs we have two pulsed light sources. In the basic characterization measurements of the PD we use pump laser pulses with a duration of 200 fs full width at half maximum (FWHM) and a center wavelength of 1340 nm. For more complex pulse pattern measurements we have developed an optical generator described in more detail in Sec. VII. The generated voltage pulses subsequently propagate along the CPW on which we placed a LiTaO₃ crystal. The electric-field-induced refractive index change in the LiTaO₃ crystal is read out using probe laser pulses with a duration of 200 fs and a center wavelength of 1550 nm [14]. Time resolution for these EOS measurements is obtained by changing the temporal delay between the pump and probe pulses. Both pulses are delivered to the chip using single mode optical fibers (SMF) ending in borosilicate ferrules. More information on the experimental setup and the fiber-chip coupling is given in Ref. [13].

The EOS is performed in two different ways. In a first realization, the LiTaO₃ crystal is glued together with the probe fiber ferrule to the sampling position on the CPW. In a second realization, the LiTaO₃ crystal is only glued to the probe fiber ferrule and this arrangement can be moved using a 3D cryogenic piezo stage. The latter allows us to perform spatially resolved EOS measurements.

In voltage pulse measurements presented in Secs. III and IV, the other end of the CPW is used to apply the DC bias to the PD via a bias tee. For the measurements presented in Secs. V the bias to the end of the CPW is replaced with the output of a Josephson Arbitrary Waveform Synthesizer (JAWS) [15], [16] and optical excitation of the PD is ceased. This allows us to measure the JAWS output propagating along the CPW exactly in the same condition employed for the measurement of voltage pulses generated from the PD. Such measurements enable calibration of the voltage pulses to a quantum standard. We use the same experimental geometry in section VI for EO measurement of temporal shape of two different JAWS output signals. The whole arrangement as depicted in Fig. 1

is inserted into a liquid He Dewar such that all measurements are done at 4 K unless otherwise noted.

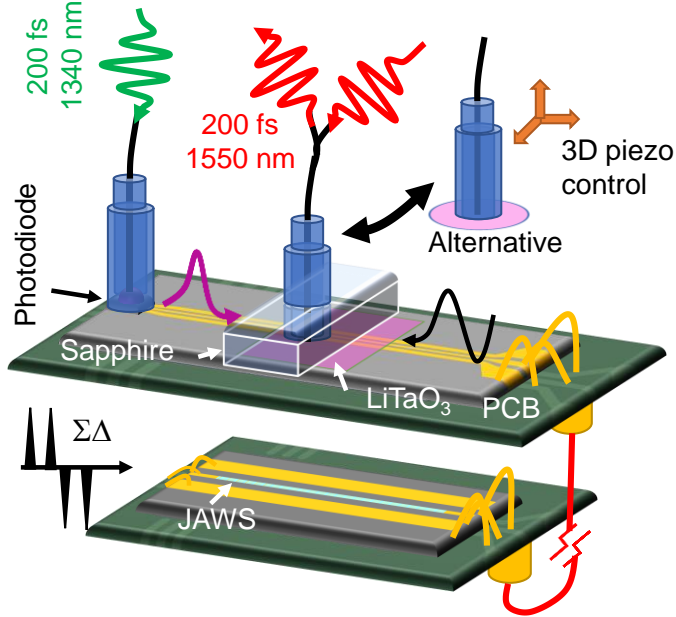


Fig. 1. Experimental scheme depicting in-situ EOS measurements of voltage pulses and JAWS synthesized signals at a cryogenic temperature. For the EOS measurements without JAWS chip, the right-hand-side of the CPW of the upper chip is terminated with a bias tee outside the chip. For visualization purposes we have simplified the output of JAWS chip, which includes additional low-pass filters across the array that are not shown in the figure.

III. CHARACTERIZATION OF FAST PHOTODIODES

As a first application example, we have used the EOS setup for the characterization of the time- and frequency response of a PD. Shown in Fig. 2(a) are the normalized time traces of voltage pulses propagating on an Au CPW measured at 4 K (solid blue) and 300 K (dashed red), obtained from a PD with a nominal bandwidth of 60 GHz. During the measurements the reverse bias U_{rev} and the photocurrent I_{ph} were kept at 1.2 V and 5 μA , respectively. We observe that both the temporal width and the tail of the voltage pulses slightly decrease when reducing the temperature from 300 K to 4 K. The reduced width of the voltage pulses and, in particular, the reduced tail are advantageous for applications in superconducting technology since it corresponds to an improvement of PD operation at cryogenic temperatures.

In Fig. 2(b) the frequency spectra corresponding to the time traces of Fig. 2(a) are shown. All

spectra extend up to ~ 250 GHz before reaching the noise level at about -60 dB below peak and the reduction of the tail in the time-domain at 4 K goes along with increased spectral components at ~ 150 GHz as compared to measurements at 300 K. A more comprehensive study in which the operation parameters like reverse bias and photocurrent were varied in a large parameter range, can be found in Ref. [10], which also includes a comparison between PDs with nominal bandwidths of 20 GHz and 60 GHz.

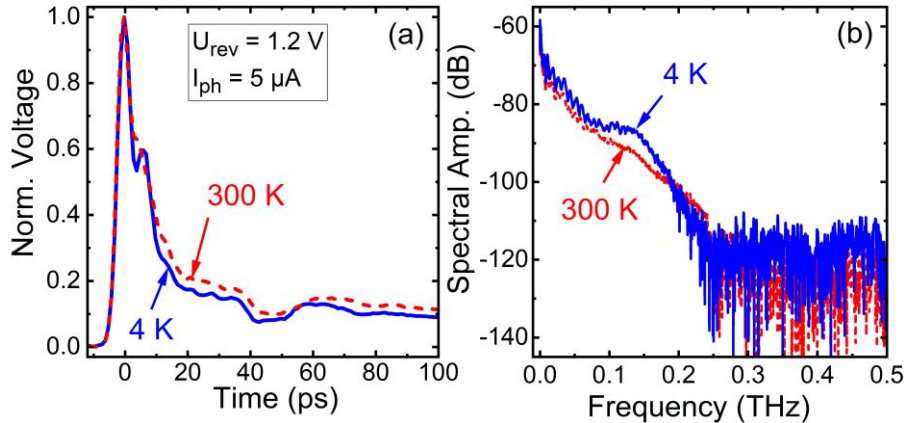


Fig. 2. (a) Temporal and (b) spectral responses of a PD with a nominal bandwidth of 60 GHz, measured by EOS on a Au CPW.

IV. REFLECTION COEFFICIENT IN SUPERCONDUCTING CIRCUITS

When performing EOS measurements over a longer time epoch it will be unavoidable that reflections from transmission line discontinuities or impedance mismatches influence the measurements. Here it should be emphasized that even CPW tapering, bond wires, or coaxial connectors lead to reflections which overlap with the incident signal. In such cases it will be essential to determine the electrical reflection coefficient at the measurement position in order to distinguish between forward and backward propagating signals.

This electrical reflection coefficient can be extracted from EOS measurements at different spatial positions on the CPW: The electrical reflection coefficient corresponds to the S_{11} scattering parameter referred to the impedance of the CPW. In our measurements we employ a CPW made from Nb with an impedance of 50Ω . Here, we like to note that in the superconducting state and at very low frequencies the impedance of the transmission line stays at 50Ω and does not become complex as compared to resistive Au transmission lines around and below 1 GHz [17].

The technique of extracting electrical reflection coefficients from two-positions measurements on a CPW has previously been demonstrated at room temperature [17], but, so far, not applied to cryogenic environments. In the following we just briefly sketch the measurement principle. More information can be found in Ref. [17]. We start with the measurement of two voltage pulses, V_1 and V_2 , at two positions on the CPW. The two measurement positions need to be at least 1 mm or 2 mm away from a transmission line discontinuity in forward direction, i.e., in the propagation direction of the voltage pulses. We then cut the measured time traces after a certain time by setting the data points at later times to zero, such that no reflection is present in the time traces. (On a typical CPW, signals propagate with a speed of approximately 1 mm/10 ps. Thus, if a transmission line discontinuity is 1 mm away from the measurement positions, the first reflection will enter the measured time window after 20 ps.). With the cut-off time traces, $V_{1,\text{cutoff}}$ and $V_{2,\text{cutoff}}$, we calculate the transfer function of the CPW between the two measurement positions in the frequency domain $p = V_{2,\text{cutoff}}/V_{1,\text{cutoff}}$. Once, p is known, the reflection coefficient Γ at the measurement position two is obtained from

$$\Gamma = \frac{V_2 - pV_1}{p(V_1 - pV_2)}, \quad (1)$$

which again denotes an equation in frequency domain.

The aforementioned scheme has been applied to the cryogenic EOS measurements in which we detect voltage pulses produced from a PD. Due to length limitations, we just present the results in the following. The blue and red lines in Fig. 3(a) show the EOS measurement at the second position on the CPW and the forward propagating signal at this position, respectively. The signals at ~ 280 ps and ~ 530 ps in the blue curve correspond to reflections from the right-hand-side end of the CPW, see Fig. 1, propagating backwards and, thus, are removed in the red curve. In contrast, the signals at ~ 420 ps and ~ 670 ps denote reflections from the left-hand side end of the CPW where the PD is flip-chip bonded, see Fig. 1. Since these reflections belong to the forward propagating voltage pulse, they are still visible in the red curve of Fig. 3(a). In Fig. 3(b) we plot the corresponding time-domain reflection coefficient, that was extracted from the measurements using Eq. (1) and used to determine the forward propagating signal. This reflection shows a large bipolar signal at ~ 140 ps. We identify the end of the Nb CPW and the bond pads/wires as the source for this reflection signal.

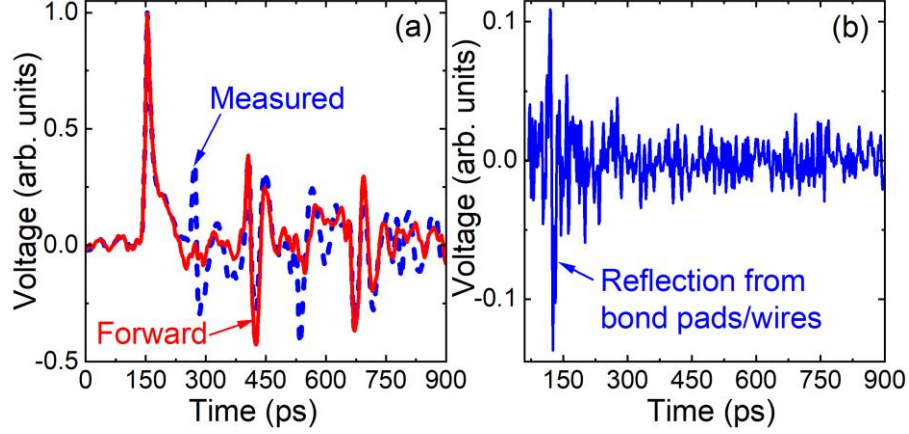


Fig. 3. (a) EOS measurement of a voltage pulse on a Nb CPW produced from a PD with a nominal bandwidth of 20 GHz. The blue and red lines show the measured signal and the forward propagating signal, respectively. (b) Reflection coefficient at the EOS position of (a). To obtain this reflection coefficient another voltage pulse was measured at a different position (not shown) and the analysis detailed in Ref. [17] was employed, see also main text.

V. CALIBRATION OF EOS MEASUREMENTS USING JAWS

In general, EOS measurements done in a pump-probe configuration yield voltage signals in arbitrary units (e.g., units of the lock-in amplifier). In such measurements the pump beam (or the signal to be measured) is amplitude-modulated and the pump-beam-induced change of the probe beam is detected with a lock-in amplifier at the modulation frequency of the pump beam. To convert these arbitrary units of the lock-in amplifier to the unit volt, one typically applies a reference signal V_{ref} with a well-known amplitude to the EOS setup [18]. The EOS response to this reference signal $V_{\text{ref,EOS}}$ then allows to convert other EOS measurements to the unit volt by a simple multiplication with $V_{\text{ref}}/V_{\text{ref,EOS}}$.

In a previous study we have shown that due to the frequency dependence of the optoelectronic devices employed for EOS, the reference signal should be equal to the modulation frequency of the optical pump beam (or of the signal to be measured). Since we modulate the pump beam in our experiment with an acousto-optic modulator at 1 MHz, we also employ a reference signal at this frequency.

To obtain direct traceability of the EOS measurements to a quantum standard, we have used a JAWS for the generation of the reference signal. Our JAWS chip comprises 3,000 Josephson junctions with a characteristic voltage $V_c = 17.3 \mu\text{V}$ and a critical current density $J_c = 93 \mu\text{A}/\mu\text{m}^2$. The JAWS chip was driven by a pulse sequence to generate a single-frequency output signal at the 1 MHz with a peak-to-peak value of 17.36 mV, see Fig. 4(a). As shown in Fig. 1 the JAWS chip was directly connected to the right-hand-side end of the CPW. The EOS response ($V_{\text{ref,EOS}}$) due to the JAWS signal (V_{ref}) was measured with the lock-in amplifier. This allowed us to calibrate voltage pulse measurements as presented in Sec. III to the unit volt. Figure 4(b) shows such a calibrated voltage pulse produced from a PD with a nominal bandwidth of 20 GHz and to the best of our knowledge this is the first EOS measurement with direct traceability of the voltage axis to a quantum standard. We will investigate in further studies how such a quantum calibration compares to previous calibration methods [18].

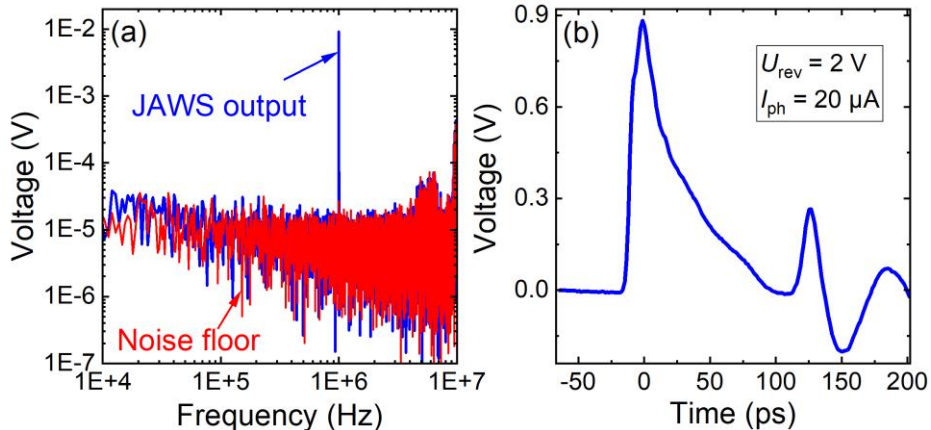


Fig. 4. (a) Spectral amplitude of the JAWS output with a single tone at 1 MHz measured with a conventional spectrum analyzer at room temperature. (b) EOS measurement of a voltage pulse on a Nb CPW produced from a strongly excited PD with a nominal bandwidth of 20 GHz. The y-axis is calibrated to the unit volt using the JAWS output.

VI. DIRECT EOS OF THE JAWS OUTPUT

In the measurements of the reference signal as discussed in the previous section, we obtained one value for $V_{\text{ref,EOS}}$, expressing the peak-to-peak value of the JAWS signal. Of course, another point of interest is the direct time-domain measurement of the JAWS signal. For this experiment we used another JAWS chip with 14,000 Josephson junctions with a characteristic voltage $V_c = 17.3 \mu\text{V}$ and a critical current density $J_c = 93 \mu\text{A}/\mu\text{m}^2$. We increased the number of Josephson junctions as

compared to the studies in Sec. V in order to increase the output voltage and, consequently, the signal-to-noise ratio of the EOS measurements.

In order to sample the output of an electrical device using our EOS platform, we have two possibilities: (i) We can synchronize the repetition rate of our probe laser to the repetition rate of the electrical device and use lock-in detection. In this case the output of the electrical device needs to be amplitude modulated at the lock-in detection frequency and time resolution is obtained by varying the time delay between the probe laser pulses and the electrical signal. (ii) We use an asynchronous sampling technique in which the repetition rate of the probe laser and the repetition rate of the electrical signal are either detuned from each other or harmonically related (but fixed otherwise). The signal can then be reconstructed by detecting each single laser pulse, if the repetition-rate difference between the probe laser and the electrical signal is exactly known [19].

For the measurements presented in this and the following section, we have used asynchronous sampling. To measure directly a JAWS waveform, we fixed the repetition rate of the probe laser to exactly 76 MHz and the frequency of the JAWS signal to exactly 1 MHz. We then adopted our data analysis such that we exactly record two periods of the JAWS signal with $2 \times 76 = 152$ data points in total. The corresponding result, displaying two periods of the 1 MHz JAWS output, is shown in Fig. 5(a). In a second measurement, we drove the JAWS with an electrical pulse pattern to produce a two-tone output with 1 MHz and 2 MHz frequency components and employed the same data analysis as before. The resulting two-period signal is shown in Fig. 5(b) and visualizes that also complex time-domain shapes can be sampled with our EOS platform.

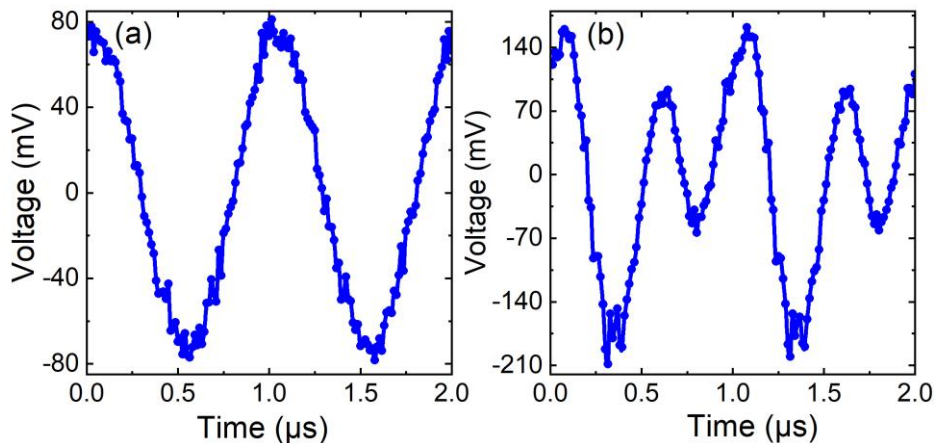


Fig. 5. EO measurement of JAWS (a) single frequency output at 1 MHz and (b) two-tone output with spectral lines at 1 MHz and 2 MHz.

VII. DIRECT EOS OF AN OPTICAL PULSE PATTERN GENERATOR

VII.1. *Optical pulse pattern generator*

Josephson arbitrary waveform generators have recently been deployed to generate signals in the GHz regime by using electrical pulse pattern generators as drivers [20]. These instruments are limited to pulses of tens of picoseconds of width. Fast pulsed lasers feeding novel optical-to-electrical converters [21] with > 100 GHz bandwidth to drive Josephson junction arrays with similarly high characteristic frequency would allow for the generation of quantized pulse patterns in an unprecedented frequency range. To test such assemblies we have built an optical femtosecond pulse generator (OPPG) that can be used to produce optical pulse clusters with freely adjustable pulse intervals and amplitudes, see Fig. 6.

The core of the OPPG is a passively mode-locked 1530-nm Er-fiber laser with a pulse repetition rate that is adjusted to be an integer multiple of the EOS frequency: $15 \times 76 \text{ MHz} = 1.14 \text{ GHz}$, see Fig. 6(a). The short, linear cavity is formed by a semiconducting saturable absorber mirror (SESAM), two lenses, a polarizer and a piece of Liekki Er80-8/125 fiber as the gain medium. Here, the intra-cavity polarizer is an essential component in the otherwise non-polarization maintaining fiber laser. Without the polarizer, the polarization will vary from pulse to pulse and even minor polarization dependence of subsequent optical components will be converted into severe amplitude noise. The dichroic output coupler mirror is directly deposited on an FC/PC fiber connector, allowing end pumping of the gain fiber (at 976 nm). The average output power is approximately 1 mW, which is increased by an order of magnitude by a pre-amplifier. The pulses are subsequently pre-chirped with a negative-dispersion fiber (NDF), amplified to about 200 mW in a normal-dispersion erbium-doped fiber amplifier [22] and recompressed to about 230 fs by five meters of standard single-mode (SM) fiber. Finally, the spectrum is broadened in a highly nonlinear fiber (HNLF) and filtered by a 12-nm bandpass filter (BPF) at 1480 nm, yielding about 5 mW average power. The filtered wavelength corresponds to the maximum responsivity of InGaAs p-i-n photodiodes at 4 K. The pulse duration after a couple of meters of additional SM fiber is around 420 fs (without dispersion compensation). The pulse repetition rate is phase-locked to the 15th harmonic of the EOS signal at 1.14 GHz by controlling the pump power. A piezo attached to the gain fiber is used to make slow adjustments to the cavity length in order to keep the average pump power at the nominal set point. Coarse repetition rate changes can be done by adjusting the cavity

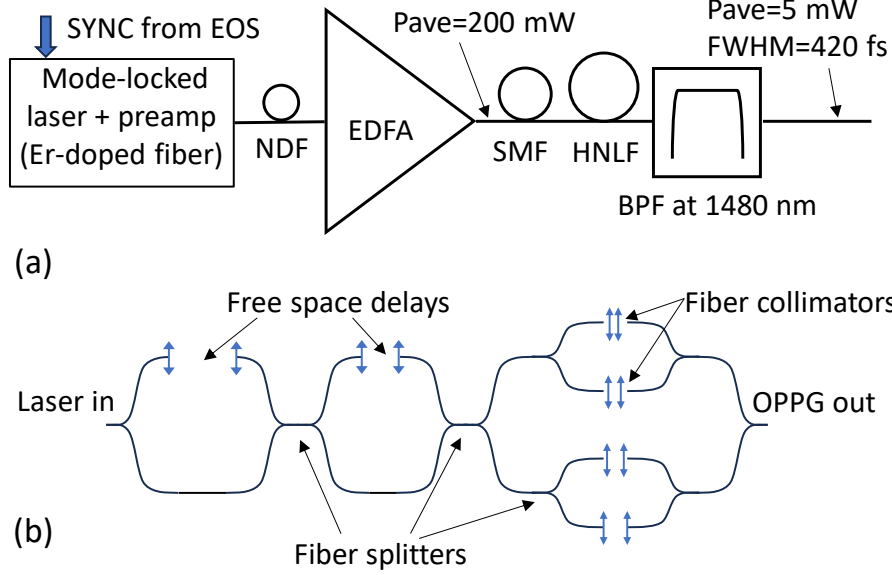


Fig. 6. (a) A custom-made femtosecond-pulse laser composed of a mode-locked fiber laser, optical amplifiers and spectral broadening section. $P_{ave} = 5$ mW of average power at 1480 nm (in the 12 nm band) is available at 1.14 GHz repetition rate. EDFA denotes an Erbium-doped fiber amplifier, NDF a negative-dispersion fiber, HNLF highly nonlinear fiber, and BPF a band-pass filter. (b) Optical pulse multiplexer based on fiber splitters, fiber collimators and free-space delay paths.

length mechanically or by adjusting the cavity temperature.

For increasing the pulse repetition rate, the pulses enter a polarization controller, a polarizer and are then fed into a polarization-maintaining fiber-optic frequency multiplier composed of 2x2 splitters and free-space delay lines leading to a pulse rate of 4.56 GHz, see Fig. 6(b). This regular pulse train is further coupled into four parallel free space delay lines, which enable adjusting the successive four pulses with any interval down to the limit when they start to overlap. Finally, we combine the interleaved pulses into a single fiber with a 4x1 splitter.

VII.2. EOS measurements

In Fig. 7 we show data measured by exciting the PD with different optical pulse trains at higher frequencies. Figure 7(a) and (b) contain EOS data with pulse-train frequencies of 4.56 GHz and 2.28 GHz, respectively. The main pulses resulting from optical excitation are clearly visible, marked with arrows. Interestingly, the background following the pulses is not stable, or periodic, in either case. This clearly demonstrates that the reflected signals from impedance mismatches are significant and must not be neglected in this short time span.

In Fig. 7(c) we show four-pulse clusters with 55 ps interval between neighboring pulses and repetition period of $1/1.14$ GHz. The signal background consisting of back and forth reflected pulses is even more pronounced than in the above cases. Obviously, this level of fidelity for driving, e.g., a JJA is not sufficient, as one needs equal amplitudes and return-to-zero pulses. Electromagnetic FEM simulations to realize proper terminations to avoid impedance mismatches are clearly needed. We like to emphasize that without our EOS method this influence of impedance mismatch on pulse clusters in a superconducting environment would not be possible.

Finally, we have performed a first attempt to measure electrical pulses directly in a JAWS chip. The characteristic frequency of Josephson junctions is 55 GHz, the critical current is $350 \mu\text{A}$, and the number of Nb-NbSi-Nb junctions in series is 100. A 60 GHz PD was flip-chip bonded directly on

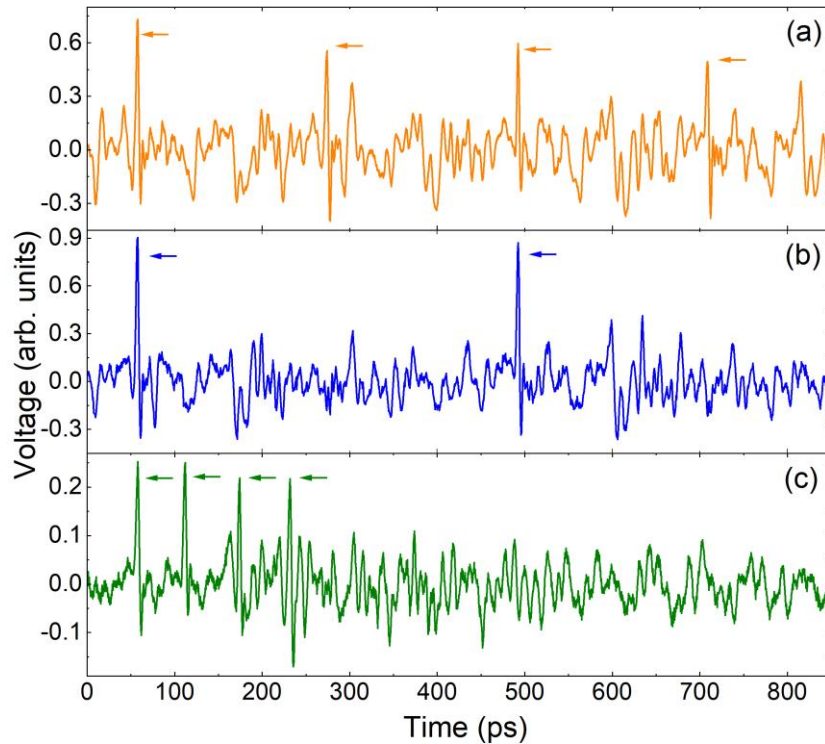


Fig. 7. EOS data measured with different optical pulse clusters used to drive a 60 GHz PD flip-chip bonded on a Nb CPW. The EOS measurement was carried out in the middle of a 13-mm long CPW between the PD and the wire-bond pads, which couple to a coaxial line in a cryoprobe. The horizontal arrows point to the temporal positions of the voltage signals generated by the optical pulse cluster. (a) 4 pulses equally spaced within a $(1.14 \text{ GHz})^{-1}$ time epoch (~ 220 ps time interval between pulses). (b) 2 pulses equally spaced within a $(1.14 \text{ GHz})^{-1}$ time epoch (~ 440 ps time interval between pulses). (c) 4 pulses equally spaced within a $(4 \times 1.14 \text{ GHz})^{-1}$ time epoch (~ 55 ps time interval between pulses).

the chip hosting the Josephson junction array. Parallel plate capacitors ($C = 27$ pF each) were fabricated in the ground lines of the CPW next to the array. The array was designed and fabricated specifically to allow EOS measurements by introducing sections of ~ 6 mm between the PD and first junction as well as between the last junction and the termination. In the first measurements, sampling was performed in the middle of the latter CPW section. The PD was illuminated with a regular pulse train at 1.14 GHz with an average photocurrent of $66 \mu\text{A}$, which corresponds to current pulses sufficiently large to transfer flux quanta. The EOS data are shown in Fig. 8. A very complex pattern with multiple peaks is observed, which results from (i) the Josephson junction array and (ii) impedance mismatch from both ends of the CPW. A detailed analysis of this pattern is beyond the scope of this paper and will be postponed to a future publication. In any case, these data demonstrate the challenges ahead in order to achieve drive patterns, where junctions are driven with ultrashort but well-separated pulses with repetition rates approaching 100 GHz.

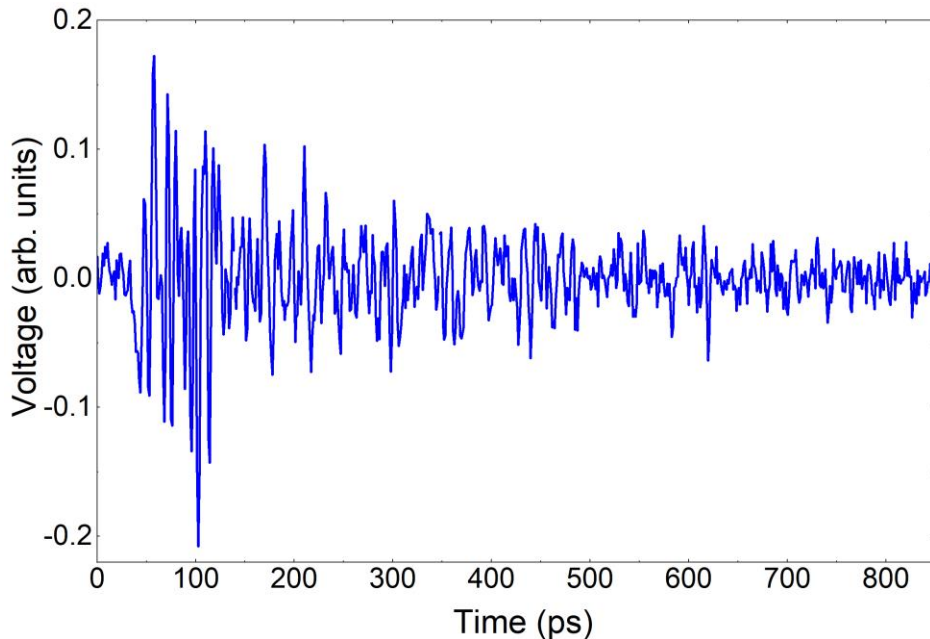


Fig. 8. EOS data obtained on a CPW between a JJA and an in-situ CPW termination. The photodiode driving the array was illuminated with optical pulses at 1.14 GHz, producing a photocurrent of $66 \mu\text{A}$.

VIII. CONCLUSIONS

We demonstrated EOS as a method for time-domain measurements of ultrafast electrical signals in cryogenic and superconducting circuits. Our results confirm the indirect observation [11] that JAWS

and JPG circuits are sensitive to transmission line effects such as reflections, especially when aiming at increasing the pulse frequencies using an OPPG. We have demonstrated a fast, optical pulse signal source suitable for driving JAWS or JPG and performed first experiments toward the time-domain measurement of quantized voltage pulses in JAWS. Furthermore, we pioneer the direct calibration of electro-optic sampling against a quantum standard and extraction of in-situ electrical reflection coefficients on a CPW in a cryogenic environment.

Our work denotes a significant step for traceable microwave measurements in superconducting circuits. While future work will concentrate on an additional uncertainty analysis, we will also analyze changes to electrical pulse patterns caused by Josephson junction arrays. We believe that such studies are essential in order to increase the output frequency of JAWS.

ACKNOWLEDGEMENT

This work was partly supported by the EMPIR programme co-financed by the Participating States and by the European Union’s Horizon 2020 research and innovation programme (grant agreement 20FUN07 SuperQuant), by the European Union’s Horizon 2020 research and innovation programme (grant agreement 899558 aCryComm), and by the German Federal Ministry of Education and Research (grant agreement 13N15934 QuMIC). In addition, funding has been received from Research Council of Finland (grants 35220/QuantLearn and 359284/Finnish Quantum Flagship) and from an internal program of VTT.

REFERENCES

- [1] P. Krantz, M. Kjaergaard, F. Yan, T. P. Orlando, S. Gustavsson, and W. D. Oliver, “A quantum engineer’s guide to superconducting qubits,” *Appl. Phys. Rev.*, vol. 6, no. 2, Art. no. 2, Jun. 2019, doi: 10.1063/1.5089550.
- [2] J. C. Bardin, D. H. Slichter, and D. J. Reilly, “Microwaves in Quantum Computing,” *IEEE J. Microw.*, vol. 1, no. 1, pp. 403–427, Jan. 2021, doi: 10.1109/JMW.2020.3034071.
- [3] D. R. Dykaar, R. Sobolewski, J. M. Chwalek, T. Y. Hsiang, and G. A. Mourou, “Electro-optic sampler for characterization of devices in a cryogenic environment,” in *Advances in Cryogenic Engineering*, Springer US, 1988, pp. 1097–1104.

- [4] C. Wang, M. Currie, D. Jacobs-Perkins, M. J. Feldman, R. Sobolewski, and T. Y. Hsiang, “Optoelectronic generation and detection of single-flux-quantum pulses,” *Appl. Phys. Lett.*, vol. 66, no. 24, pp. 3325–3327, Jun. 1995, doi: 10.1063/1.113745.
- [5] M. Griebel *et al.*, “Picosecond sampling with fiber-illuminated ErAs:GaAs photoconductive switches in a strong magnetic field and a cryogenic environment,” *Appl. Phys. Lett.*, vol. 82, no. 19, pp. 3179–3181, May 2003, doi: 10.1063/1.1573367.
- [6] F. Lecocq, F. Quinlan, K. Cicak, J. Aumentado, S. A. Diddams, and J. D. Teufel, “Control and readout of a superconducting qubit using a photonic link,” *Nature*, vol. 591, no. 7851, pp. 575–579, Mar. 2021, doi: 10.1038/s41586-021-03268-x.
- [7] M. J. Weaver *et al.*, “An integrated microwave-to-optics interface for scalable quantum computing,” *Nat. Nanotechnol.*, vol. 19, no. 2, pp. 166–172, Feb. 2024, doi: 10.1038/s41565-023-01515-y.
- [8] M. A. Castellanos-Beltran *et al.*, “Coherence-limited digital control of a superconducting qubit using a Josephson pulse generator at 3 K,” *Appl. Phys. Lett.*, vol. 122, no. 19, p. 192602, May 2023, doi: 10.1063/5.0147692.
- [9] A. J. Sirois, M. Castellanos-Beltran, A. E. Fox, S. P. Benz, and P. F. Hopkins, “Josephson Microwave Sources Applied to Quantum Information Systems,” *IEEE Trans. Quantum Eng.*, vol. 1, pp. 1–7, 2020, doi: 10.1109/TQE.2020.3045682.
- [10] S. Priyadarshi *et al.*, “Cryogenic Fiber-coupled Electro-optic Characterization Platform for High-speed Photodiodes,” *J. Infrared Millim. Terahertz Waves*, vol. 45, no. 1–2, pp. 159–170, 2024, doi: 10.1007/s10762-024-00966-1.
- [11] J. Nissilä *et al.*, “Driving a low critical current Josephson junction array with a mode-locked laser,” *Appl. Phys. Lett.*, vol. 119, no. 3, p. 032601, Jul. 2021, doi: 10.1063/5.0060804.
- [12] C. A. Donnelly *et al.*, “Quantized Pulse Propagation in Josephson Junction Arrays,” *IEEE Trans. Appl. Supercond.*, vol. 30, no. 3, pp. 1–8, Apr. 2020, doi: 10.1109/TASC.2019.2929481.
- [13] S. Priyadarshi *et al.*, “In-situ electro-optic sampling of microwave signals applied to superconducting circuits,” in *2024 Conference on Precision Electromagnetic Measurements (CPEM)*, Jul. 2024, pp. 1–2. doi: 10.1109/CPEM61406.2024.10646099.
- [14] G. Gallot and D. Grischkowsky, “Electro-optic detection of terahertz radiation,” *J Opt Soc Am B*, vol. 16, no. 8, p. 1204, 1999.
- [15] O. Kieler *et al.*, “Optical Pulse-Drive for the Pulse-Driven AC Josephson Voltage Standard,” *IEEE Trans. Appl. Supercond.*, vol. 29, no. 5, p. 1200205, 2019, doi: 10.1109/TASC.2019.2899851.

- [16] O. Kieler, R. Behr, R. Wendisch, S. Bauer, L. Palafox, and J. Kohlmann, “Towards a 1 v Josephson arbitrary waveform synthesizer,” *IEEE Trans. Appl. Supercond.*, vol. 25, no. 3, pp. 1–5, 2015, doi: 10.1109/TASC.2014.2366916.
- [17] M. Bieler, H. Füsler, and K. Pierz, “Time-Domain Optoelectronic Vector Network Analysis on Coplanar Waveguides,” *IEEE Trans. Microw. Theory Tech.*, vol. 63, no. 11, pp. 3775–3784, 2015, doi: 10.1109/TMTT.2015.2481426.
- [18] P. Struszewski and M. Bieler, “Quantitative electro-optic measurements of ultrafast electrical signals on planar transmission lines: Pitfalls and caveats,” in *2020 Conference on Precision Electromagnetic Measurements (CPEM)*, Denver, CO, USA: IEEE, 2020, pp. 1–2. doi: 10.1109/CPEM49742.2020.9191725.
- [19] P. Struszewski and M. Bieler, “Asynchronous Optical Sampling for Laser-Based Vector Network Analysis on Coplanar Waveguides,” *IEEE Trans. Instrum. Meas.*, vol. 68, no. 6, pp. 2295–2302, Jun. 2019, doi: 10.1109/TIM.2018.2880052.
- [20] C. A. Donnelly *et al.*, “1 GHz Waveform Synthesis With Josephson Junction Arrays,” *IEEE Trans. Appl. Supercond.*, vol. 30, no. 3, Art. no. 3, Apr. 2020, doi: 10.1109/TASC.2019.2932342.
- [21] S. M. Koepfli *et al.*, “Metamaterial graphene photodetector with bandwidth exceeding 500 gigahertz,” *Science*, vol. 380, no. 6650, pp. 1169–1174, Jun. 2023, doi: 10.1126/science.adg8017.
- [22] K. Tamura and M. Nakazawa, “Pulse compression by nonlinear pulse evolution with reduced optical wave breaking in erbium-doped fiber amplifiers,” *Opt. Lett.*, vol. 21, no. 1, pp. 68–70, Jan. 1996, doi: 10.1364/OL.21.000068.